

# Electronic theory of ultrafast spin dynamics

C. Li,\* G. Lefkidis, and W. Hübner

*Department of Physics and Research Center OPTIMAS,  
Kaiserslautern University of Technology  
PO Box 3049, 67653, Kaiserslautern, Germany*

(Dated: 25.11.2008)

NiO is a good candidate for ultrafast magnetic switching because of its large spin density, antiferromagnetic order, and clearly separated intragap states. In order to detect and monitor the switching dynamics, we develop a systematic approach to study optical second harmonic generation (SHG) in NiO, both at the (001) surface and in the bulk. In our calculations NiO is modeled as a doubly embedded cluster. All intragap  $d$ -states of the bulk and the (001) surface are obtained with highly-correlational quantum chemistry and propagated in time under the influence of a static magnetic field and a laser pulse. We find that demagnetization and switching can be best achieved in a subpicosecond regime with linearly rather than circularly polarized light. We also show the importance of including an external magnetic field in order to distinguish spin-up and spin-down states and the necessity of including magnetic-dipole transitions in order to realize the  $\Lambda$ -process in the centrosymmetric bulk. Having already shown the effects of phonons in the SHG for the bulk NiO within the frozen-phonon approximation, and following the same trail of thoughts, we discuss the role of phonons in a fully quantized picture as a symmetry-lowering mechanism in the switching scenario and investigate the electronic and lattice temperature effects.

PACS numbers: 78.68.+m, 78.47.+p, 73.20.-r, 78.20.Ls

## I. INTRODUCTION

In recent decades there has been a continuous strain to minimize as much as possible the time needed to record data on magnetic materials. At the same time, the tremendous increase in storage density and read-write speed in magnetic storage media is reaching its physical limits. Ever since the light-induced demagnetization of ferromagnets was discovered<sup>1</sup>, several light-driven scenarios and mechanisms have been proposed<sup>2,3</sup>, and it has already been demonstrated that exploiting the ultrafast electron-photon interaction can lead to subpicosecond dynamics<sup>4</sup>. Furthermore, it has been experimentally assessed that the electronic excitations can non-thermally control spin dynamics<sup>5</sup> and magnetic phases<sup>6</sup> in magnetic materials. Laser manipulation has been well understood in atomic and molecular systems, which stimulates the demand for an implementation of these mechanisms in practical device applications. Thus, the investigation of electron and spin dynamics in the bulk, surfaces, and nanostructures of nonmagnetic as well as magnetic materials has attracted considerable interest in recent years.

Nonlinear optics is more selective than nonlocal linear optics, making it an ideal tool for investigating antiferromagnets. NiO is a good candidate for such a scenario due to its large spin density, antiferromagnetic (AF) order, and clearly separated intragap states. Although bulk NiO possesses a center of inversion, it generates a second harmonic signal<sup>7</sup>. In the literature there are to date four main explanations for its origin (i) spin-orbit coupling (SOC), (ii) a signal that mainly results from the surface, (iii) inclusion of higher order transitions, and (iv) lowering of the crystallographic symmetry due to local distortions or phonons. Recent works<sup>8,9</sup> from our group showed that explanations (i) and (iii), especially the latter, are the most probable candidates for the physics behind. The first two explanations are also demonstrated by a recent experi-

ment<sup>10</sup>.

In this paper, we review our studies on electronic theory of ultrafast spin dynamics in recent years. The remainder of this paper is organized as follows. In Sec. 2, we introduce quantum chemistry methods used in the calculations. In Sec. 3, we include SOC. In Sec. 4, second harmonic generation (SHG) is calculated. Symmetry analysis of the contributions to the second order susceptibility tensors ( $\chi^{(2)\omega}$ ) is performed. In Sec. 5, we show the effects of phonons as a symmetry-lowering mechanism in the switching scenario. In Sec. 6, we present our final results for realization of spin manipulation. Finally, in Sec. 7, we present our summary and outlook for future work.

## II. QUANTUM CHEMISTRY

One can use either the real or the momentum space approach to model both the surface and the bulk of NiO. Their major difference is that only the first one is able to find the localized intragap  $d$ -states of the Ni ion. These dispersionless states are experimentally confirmed for the surface<sup>11,12</sup> and for the bulk<sup>13</sup>. Although some previous calculations with extended local density approximation (LDA++) within the Hubbard-I approach<sup>14</sup> and within the  $GW$  approximation<sup>15,16,17</sup> give better results for the gap than the real space approach, and a recent calculation combining LDA and dynamical mean-field theory provides an accurate band structure of NiO<sup>18</sup>, they persistently miss the intragap states. Additionally, correlations play an important role in NiO, and the real space approach is therefore more suitable to describe its complex electronic structure. Last but not least we wish not only to calculate the energy levels but the wavefunctions.

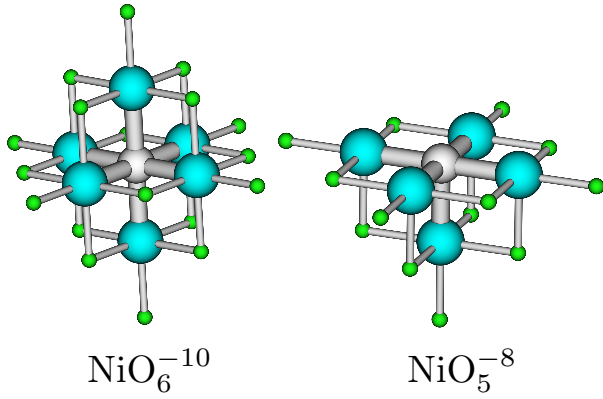


FIG. 1: Clusters used for the bulk (left) and the surface (right). Large dark spheres represent oxygen atoms, the central grey sphere the nickel atom, and the small spheres the surrounding effective core potentials.

### A. Doubly embedded cluster

In order to model the system we use a doubly embedded cluster<sup>8,19</sup>. For the surface a  $\text{NiO}_5^{-8}$  cluster is used and for the bulk a  $\text{NiO}_6^{-10}$  cluster. Both clusters are first embedded in a shell of effective core potentials (ECP), that account for the electrostatic properties of the Ni ions in the immediate vicinity (Fig. 1). The whole structure is then again embedded in a charge point field (CPF) which describes the surrounding Madelung potential.

### B. Computational levels

We use several correlation levels in the calculations, mainly for comparison and checking reasons, such as configuration interaction (CI) with single excitations (CIS), single and double excitations (CISD), single excitations with energy contributions from higher excitations [CIS(D)]<sup>20</sup>, quadratic configuration interaction (QCI), with singles (QCIS), doubles (QCISD), and doubles with higher excitation energy contributions (QCISD-T). A method well suited to describe all  $d$ -states is the multiconfigurational complete active space configuration interaction (MC-CAS or CASSCF), which can describe each state separately and can include dynamical correlations as well<sup>21</sup>. Table I shows some results of  $\text{NiO}_5^{-8}$  from different correlation levels.

## III. SPIN-ORBIT COUPLING

The SOC, characterized by the interaction between the electron spin moment and the orbital angular momentum, results in an additional effect of splitting of the electron energy levels. The high-quality linear and nonlinear (SHG) optical spectra of NiO given by Fiebig *et al.*<sup>7</sup> provide a good chance to directly compare the experimental and theoretical details of the fine structure.

Using the CIS method and including SOC, we concentrate on the 21 lowest triplet states originating from the crystal field and spin-orbit splitting of the  ${}^3F$  level of the  $\text{Ni}^{2+}$  ion. Symmetry analysis shows that SOC does not split the singlet states. It shifts, however, their energy due to the admixture of the triplet states. As a consequence some singlet-triplet transitions become allowed.

Figure 2 in reference<sup>9</sup> shows the calculated fine structure of bulk NiO. Including SOC leads to a slight lowering of the ground state energy. The splitting of the second excited state ( $\Delta E_{3\Gamma_5^+} = E_{\Gamma_2^+} - E_{\Gamma_3^+} = 71$  meV) ( ${}^3\Gamma_5^+$ ) is in good agreement with the most accurate measurements (around 70 meV) of the optical absorption and SHG spectra of NiO<sup>7</sup>. In addition, our transition  ${}^3\Gamma_5^+ \rightarrow {}^3\Gamma_2^+$  at about 0.9 eV agrees well with the SHG structure around 1.0 eV by Fiebig *et al.*<sup>7</sup>.

We have also found that the splitting of energies leads to additional electric dipole (ED) transitions, which corresponds to the SHG response that can be observed when SOC is taken into account.

## IV. SECOND HARMONIC GENERATION

### A. Theory

When we consider a monochromatic plane wave interacting with a material, it induces a response which leads to a source term in the Maxwell equations. Expanding its inhomogeneous solution yields terms of the polarization ( $\mathbf{P}_s$ ), the magnetization ( $\mathbf{M}_s$ ), and the electric quadrupole (EQ) polarization ( $\vec{Q}_s$ ), which are functions of the incident field<sup>23,24</sup>. Taking into account no more than one second-order transition and considering the indistinguishability of the two incident photons, we have

$$\begin{pmatrix} \mathbf{P}_s \\ \mathbf{M}_s \\ \vec{Q}_s \end{pmatrix} \propto \begin{pmatrix} \overleftrightarrow{\chi}^{eee} & \overleftrightarrow{\chi}^{eem} & \overleftrightarrow{\chi}^{eeq} \\ \overleftrightarrow{\chi}^{mee} & 0 & 0 \\ \overleftrightarrow{\chi}^{qee} & 0 & 0 \end{pmatrix} \cdot \begin{pmatrix} \mathbf{E}\mathbf{E} \\ \mathbf{E}\mathbf{H} \\ \mathbf{E}\vec{Q} \end{pmatrix} \quad (1)$$

In the right side, the two last upper indices denote the nature of the two absorptions, while the first one the nature of the emissions [ $e$  for ED,  $m$  for magnetic dipole (MD), and  $q$  for EQ induced transitions], and the lower indices in the subsequent formulas represent the directions of the corresponding multipoles. To calculate  $\overleftrightarrow{\chi}^{(2\omega)}$ , adopting the Coulomb gauge, neglecting the  $\mathbf{A}^2$  term (this term leads to a tensor completely analogous to the nonlinear optical conductivity tensor  $\overleftrightarrow{\Sigma}^C$  discussed by Andersen *et al.*<sup>25</sup>) and setting  $\mathbf{n}$  and  $\mathbf{a}$  as the unit vectors in the propagation and the polarization direction of the light beam respectively, we get a perturbation term, a Taylor expansion of which keeping only the first two terms in  $i\frac{\omega}{c}\mathbf{n} \cdot \mathbf{r}$  yields for the interaction elements:

$$V'_{ij} \simeq -\frac{e\omega_{ij}\mathcal{E}}{\omega}d_{ij}^{\mathbf{a}} - \frac{e\mathcal{B}}{2m_e c}L_{ij}^{\mathbf{a} \times \mathbf{n}} - \frac{e\omega_{ij}\nabla \cdot \mathcal{E}}{2\omega}Q_{ij}^{\mathbf{a}, \mathbf{n}} \quad (2)$$

where  $\mathcal{E}$  and  $\mathcal{B}$  are magnitudes of the electric and magnetic fields, respectively,  $\omega$  is the frequency of the incident light,

TABLE I:  $d$ -state and gap energies (in eV) at various correlation levels of the  $\text{NiO}_5^{-8}$  cluster<sup>22</sup>.

$\text{NiO}_5^{-8}$	HF	<sup>3</sup> CIS	<sup>3</sup> CIS(D)	<sup>1</sup> CIS	CCSD	QCISD(T)	CAS	exp. <sup>a</sup>	$\text{NiO}_5^{-8}$	CAS
<sup>1</sup> B <sub>1</sub>	0.00	0.00	0.00	0.00	0.00	0.00	0.00	0.0	<sup>1</sup> B <sub>1</sub>	2.15
<sup>1</sup> E	0.50	0.53	0.59	0.78	0.56	0.56	0.49	0.6	<sup>2</sup> <sup>1</sup> A <sub>1</sub>	3.49
<sup>1</sup> B <sub>2</sub>	0.93	2.00	1.74	–	1.14	1.17	0.92	1.1	<sup>2</sup> <sup>1</sup> E	3.93
<sup>1</sup> A <sub>2</sub>	1.93	0.97	1.16	1.85	1.38	1.26	1.06	1.3	<sup>3</sup> <sup>1</sup> A <sub>1</sub>	4.20
<sup>2</sup> <sup>3</sup> E	1.73	–	–	–	1.68	1.54	1.25	–	<sup>2</sup> <sup>1</sup> B <sub>1</sub>	4.22
<sup>1</sup> A <sub>1</sub>	2.79	–	–	2.61	1.47	1.26	1.82	–	<sup>3</sup> <sup>1</sup> E	4.23
<sup>1</sup> E	5.12	–	–	2.82	3.10	-4.75	2.51	2.1	<sup>2</sup> <sup>1</sup> B <sub>2</sub>	4.35
<sup>1</sup> B <sub>2</sub>	4.30	–	–	2.24	2.84	1.76	2.94	–	<sup>4</sup> <sup>1</sup> A <sub>1</sub>	8.29
<sup>2</sup> <sup>3</sup> A <sub>2</sub>	1.94	–	–	–	1.79	1.60	2.95	–	–	–
<sup>1</sup> A <sub>2</sub>	4.71	–	–	3.01	3.07	-2.69	3.15	–	–	–
<sup>3</sup> <sup>3</sup> E	–	2.85	2.77	–	–	–	3.40	–	–	–
Gap	7.19	7.64	5.57	10.76	–	–	7.56	–	–	–

<sup>a</sup> Taken from Ref. 11.

$d_{ij}^a$ ,  $L_{ij}^{a \times n}$  and  $Q_{ij}^{a,n}$  are the components of the ED, MD, and EQ transitions along the directions indicated by the superscripts. The microscopic formulas for  $\overleftrightarrow{\chi}^{(2\omega)}$ , derived from the Liouville equation of motion, by applying second order perturbation theory<sup>19,24,26</sup>, has already been given<sup>8,21</sup>

$$\chi_{xyz}^{ijk} \propto \sum_{\alpha\beta\gamma} \left[ V_{\gamma\alpha}^{i,x} \overline{V_{\alpha\beta}^{j,y} V_{\beta\gamma}^{k,z}} \times \frac{f(E_\gamma) - f(E_\beta)}{E_\gamma - E_\beta - \hbar\omega + i\hbar\Gamma} - \frac{f(E_\beta) - f(E_\alpha)}{E_\beta - E_\alpha - \hbar\omega + i\hbar\Gamma} \right], \quad (3)$$

where the indices  $i, j, k$  denote the nature of the transition (i.e.,  $e$  for ED,  $m$  for MD, and  $q$  for EQ transitions) between states  $\alpha$  and  $\beta$ , and  $f(E)$  is the population distribution function. The overbar means symmetrization with respect to the two incident photons.

## B. Symmetry analysis

Our cluster is in the ferromagnetic phase due to the model involving only one Ni atom. The real space approach is not

---

and

$$\overleftrightarrow{\chi}_{C_{4v}}^{eem} = \left( \begin{array}{ccc|ccc} 0 & 0 & 0 & \chi_{xyz}^{eem} & 0 & 0 \\ 0 & 0 & 0 & 0 & -\chi_{xzy}^{eem} & 0 \\ 0 & 0 & 0 & 0 & 0 & \chi_{zxy}^{eem} \end{array} \right) \quad (6)$$

with three, one, and three independent matrix elements, respectively. Symmetrizing results in the vanishing of the  $\chi_{zxy}^{eem}$  element, in the  $O_h$  point group (bulk) we further have  $\chi_{xyz}^{eem} = -\chi_{xzy}^{eem}$  and thus the whole tensor disappears.

The tensors are of rank four when involving EQ transitions. Symmetrizing with respect to the last two indices can simplify

able to describe the translational invariance of the real crystal lattice and the different domains, which give different second harmonic signals<sup>27,28</sup>.

The  $\text{NiO}_5^{-8}$  cluster has a  $C_{4v}$  symmetry with no inversion center, and therefore all rank three tensors are allowed, and their symmetrized forms are

$$\overleftrightarrow{\chi}_{C_{4v}}^{eee} = \left( \begin{array}{ccc|ccc} 0 & 0 & 0 & 0 & \chi_{xxz}^{eee} & 0 \\ 0 & 0 & 0 & \chi_{xxz}^{eee} & 0 & 0 \\ \chi_{zxx}^{eee} & \chi_{zxx}^{eee} & \chi_{zzz}^{eee} & 0 & 0 & 0 \end{array} \right), \quad (4)$$

$$\overleftrightarrow{\chi}_{C_{4v}}^{mee} = \left( \begin{array}{ccc|ccc} 0 & 0 & 0 & \chi_{xyz}^{mee} & 0 & 0 \\ 0 & 0 & 0 & 0 & -\chi_{xyz}^{mee} & 0 \\ 0 & 0 & 0 & 0 & 0 & 0 \end{array} \right), \quad (5)$$

---

the  $\overleftrightarrow{\chi}^{qee}$  tensor both for the bulk and for the surface,  $\chi_{(ij)kl}^{qee}$  has nine nonvanishing contributions. For the group  $O_h$  we are treating with a  $T_4$  tensor<sup>29</sup> with three independent elements, the symmetrized form is

$$\chi_{O_h}^{qee} = \begin{pmatrix} \chi_{(x^2-y^2)xx}^{qee} & \chi_{(x^2-y^2)xx}^{qee} & 0 & 0 & 0 & 0 \\ \chi_{(z^2)xx}^{qee} & \chi_{(z^2)xx}^{qee} & \chi_{(x^2-y^2)xx}^{qee} + \chi_{(z^2)xx}^{qee} & 0 & 0 & 0 \\ 0 & 0 & 0 & \chi_{(xy)xy}^{qee} & 0 & 0 \\ 0 & 0 & 0 & 0 & \chi_{(xy)xy}^{qee} & 0 \\ 0 & 0 & 0 & 0 & 0 & \chi_{(xy)xy}^{qee} \end{pmatrix}. \quad (7)$$

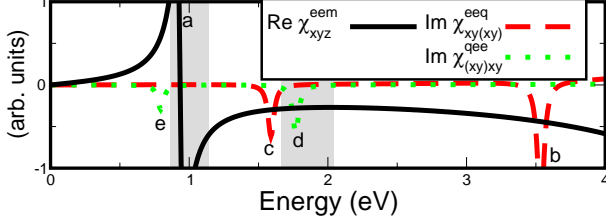


FIG. 2: Tensor elements of the bulk of NiO. Peak *a* corresponds to transition  $1^3A_{2g} \leftrightarrow 1^3T_{2g}$  with frequency  $\omega$ , peak *b* to  $1^3A_{2g} \leftrightarrow 2^3T_{1g}$  with frequency  $\omega$ , peak *c* to  $1^3A_{2g} \leftrightarrow 1^3T_{1g}$  with frequency  $\omega$ , peak *d* to  $1^3A_{2g} \leftrightarrow 2^3T_{1g}$  with frequency  $\omega$  and peak *e* to  $1^3A_{2g} \leftrightarrow 1^3T_{1g}$  with frequency  $2\omega$ .

Furthermore we have also analyzed, using group theory, the contributions to the  $\chi^{(2\omega)}$  arising from magnetic domains rotated with respect to each other<sup>27</sup>. In addition, a similar symmetry analysis has been performed for ferromagnetic systems to obtain the nonlinear susceptibility tensor by Andersen *et al.* where even and odd contributions are attributed to spin-dependent transitions<sup>30</sup>.

### C. Results

Altogether there are three types of independent tensor elements, namely  $\chi_{xyz}^{eem}$ ,  $\chi_{xy(xy)}^{eeq}$ , and  $\chi_{(xy)xy}^{qee}$ <sup>29</sup>, in bulk NiO. The most distinct peak at 0.94 eV (Fig. 2) due to the MD transitions perfectly coincides with the experimental results<sup>7</sup>. Peak *d*, which arises from an EQ transition, also agrees very well. Further splitting of these peaks can easily be attributed to SOC and/or phonons.

Considering certain experimental conditions, we repopulate the states in two ways<sup>21</sup>, that is, an energetically balanced way which consists of an equal distribution of electrons in all sub-levels with a given energy, and an energetically nonbalanced way where anisotropy is included at the same time, as demonstrated in Figures 3 and 4. The first case could happen when a system is prepared with an unpolarized pump laser pulse, and the results show that higher kinetic temperatures would result in excitations to different states. In the second way, which could happen with a polarized pump beam,  $\chi_{yz}^{eem}$  shows the same behavior as in the thermal distribution, while  $\chi_{xyz}^{eem}$  exhibits additional symmetry violating features.

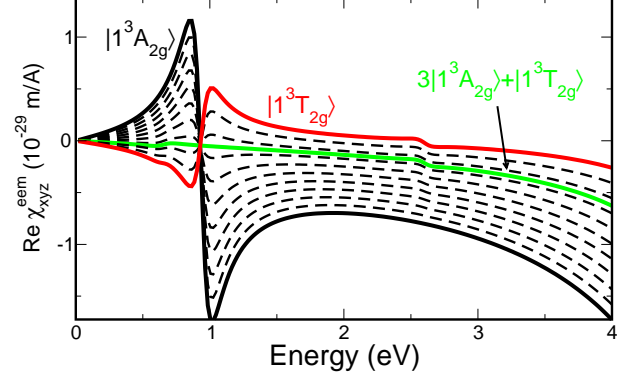


FIG. 3: Energetically balanced repopulation of the  $\text{NiO}_6^{-10}$  cluster and its effect on the  $\chi_{xyz}^{eem}$  tensor element. The outer solid lines (black and red) represent the tensor element for fully populated ground and first excited state, the inner solid line (green) the suppressed peak when the population ratio equals 3:1.

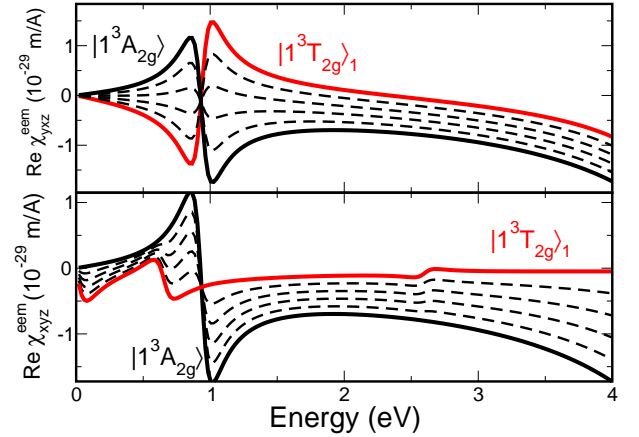


FIG. 4: Energetically nonbalanced repopulation of the  $\text{NiO}_6^{-10}$  cluster and its effect on the  $\chi_{xyz}^{eem}$  and  $\chi_{yz}^{eem}$  tensor elements.

## V. PHONONS

### A. Frozen-phonon approximation

Up to now, we supposed a non-distorted lattice, which of course is not true in the real system. However, the system deviates from the full  $O_h$  symmetry through the static lattice distortion along the  $\langle 111 \rangle$  axis due to spin ordering or dynamic distortions like phonons. Here we consider the latter

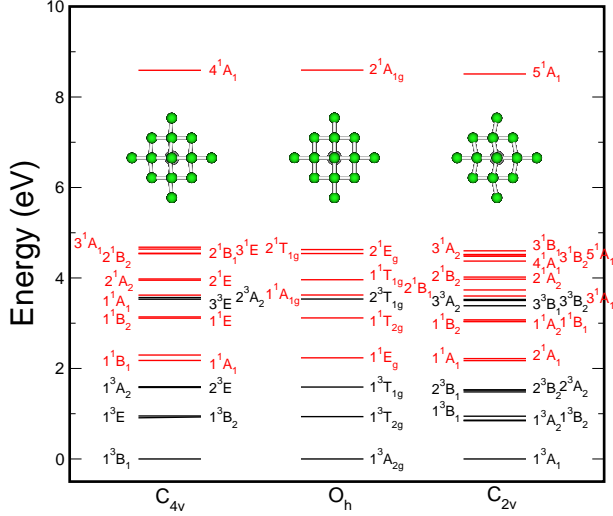


FIG. 5: In the middle panel are the calculated levels for  $O_h$  symmetry, on the left for  $C_{4v}$  and on the right for  $C_{2v}$ . The insets show the respective clusters (with the effective charge points).

case, which takes place both in the bulk and the surface. We treat the electronic movements quantum mechanically within the Born-Oppenheimer approximation while the motion of the nuclei is considered to happen on a much slower pace, giving time to the electrons to adiabatically follow them.

The optical phonons lower the local symmetry of the  $NiO_6^{-10}$  in our rocksalt structure, even at the  $\Gamma$  point. There are a few cases, however, where the local geometry on any Ni site is the same throughout the crystal, the level splittings of which are shown in Fig. 5.

Now SHG becomes possible even within the ED approximation since the inversion symmetry is broken. Fig. 6 depicts the  $\chi^{eee}$  and the  $\chi^{eem}$  tensor elements in the  $NiO_6^{-10}$  cluster for a phonon coordinate of 3% displacement, at the  $\Gamma$  point, when the symmetry on every Ni site is  $C_{4v}$ . Here, the energy splitting of the peak near 1 eV of the  $\chi^{eem}$  (about 5 meV) is very close to the experimental splitting of the first intense SHG peak observed by Fiebig *et al.*<sup>7</sup>.

A lower symmetry will lead to an even richer structure<sup>21</sup>. Note that generally the triply degenerate states get split into three levels, but two of which are always almost degenerate in energy, and thus the peaks get split into two peaks and not three, as shown in Fig. 7.

## B. Time evolution

The calculations show that the relation between  $\chi^{(2\omega)}(\mathbf{q})$  and  $\mathbf{q}$  is not linear (Fig. 7). Nonetheless, since in our approximation we consider SHG to be instantaneous we calculate the time average over a whole period of  $(\chi^{(2\omega)})^2$  as shown in Fig. 8. We consider a simple harmonic model (uncoupled phonons), and take snapshots for amplitude of up to 3% lattice displacement with a step of 0.25%. It is found that the peaks do not get broadened but split, and the intensity of the peaks

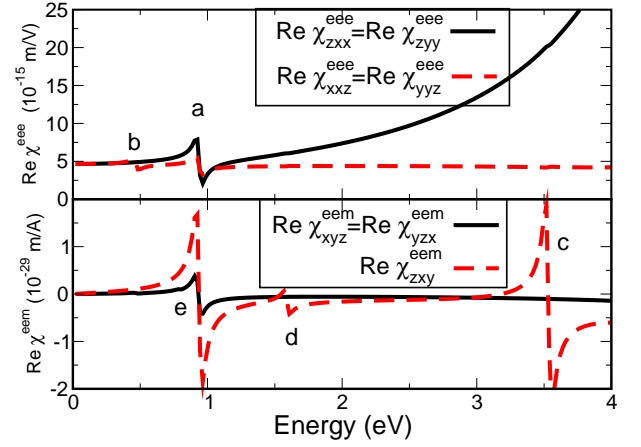


FIG. 6:  $\chi^{eee}$  and  $\chi^{eem}$  tensors for the  $NiO_6^{-10}$  in the case of the  $\Gamma$  point of one optical phonon along the  $z$  direction ( $C_{4v}$  symmetry). Note that peaks  $a$  and  $e$  are shifted with respect to each other by 5 meV, a splitting which is visible only if zoomed in.

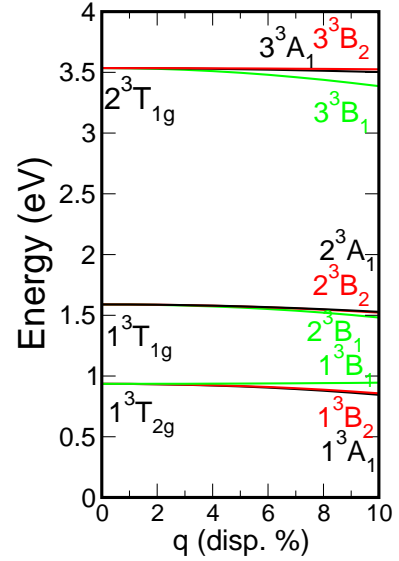


FIG. 7: Splitting of the levels vs. displacement in the case of the transversal plane wave (see text) along the  $z$  direction ( $C_{2v}$  symmetry). The splitting is an even function of  $\mathbf{q}$ .

has an almost quadratic relationship to the amplitude of the displacement. The time resolved results shown in Fig. 9 and Fig. 10 exhibit the relationship between the tensor elements ( $\chi_{xxz}^{eee}$  and  $\chi_{xyz}^{eem}$ ) and the phononic coordinate  $\mathbf{q}$ . Both the behaviors are clearly nonlinear, and one can distinguish three regimes<sup>21</sup>. A similar behavior can be observed for the  $\chi_{xyz}^{mee}$  tensor element.

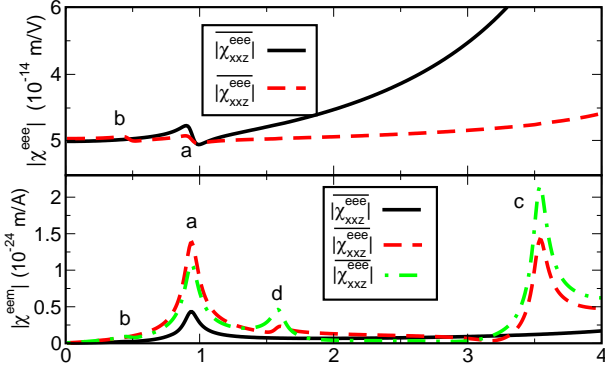


FIG. 8: Time averaged  $|\hat{\chi}^{eee}|$  and  $|\hat{\chi}^{em}|$  tensors for the  $\text{NiO}_6^{-10}$  in the case of the  $\Gamma$  point of one optical phonon along the  $z$  direction ( $C_{4v}$  symmetry) with an lattice displacement of amplitude of 3%.

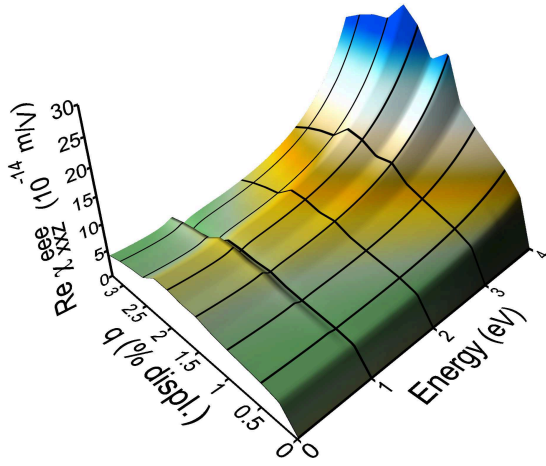


FIG. 9:  $\chi_{xxxz}^{eee}$  vs. photon energy and vs.  $\mathbf{q}$ . A peak starts appearing after  $\mathbf{q} = 0.25\%$  at energy  $\sim 0.95$  eV.

## VI. SPIN MANIPULATION

### A. Simple models for laser-induced dynamics

We start our investigations of the spin manipulation with the simplest two-level and three-level systems<sup>31</sup>. To obtain a spin mixed state, two excited states of definite (and opposite) spin are needed, which are mixed through SOC. Thus, the minimum scenario for optically induced spin dynamics is a four-level system: two almost degenerate pure spin states at low energy (ground states) and two also almost degenerate states at high energy which can be mixed by SOC<sup>32</sup>.

### B. Ultrafast magnetic switching in NiO

Based on the above suggested four-level system, we present an ultrafast magneto-optical switching mechanism in NiO. Fig. 11 shows the population evolution of the lowest levels

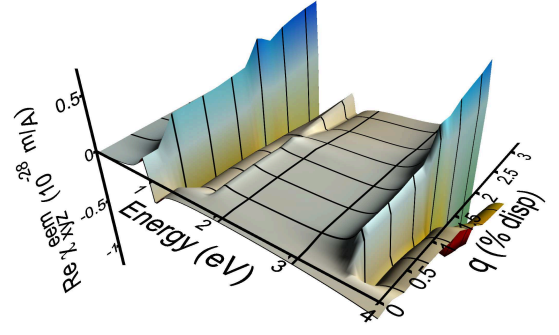


FIG. 10:  $\chi_{xyz}^{em}$  vs. photon energy and vs.  $\mathbf{q}$ . Two new peaks appear after  $\mathbf{q} = 0.25\%$ , one at energy  $\sim 1.590$  eV which changes its phase at  $\mathbf{q} = 2.0\%$ , and one at energy  $\sim 3.65$  eV.

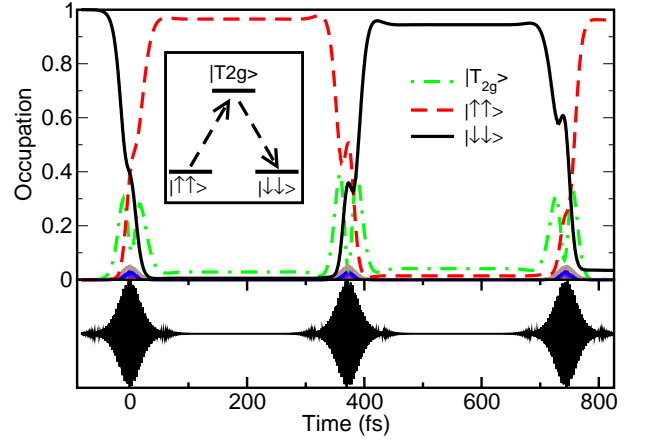


FIG. 11: Top: population evolution of the lowest lying levels in bulk of NiO. Bottom: Laser profile.

in bulk NiO and the corresponding laser profile. In order to achieve switching we have to choose a suitable mixed-spin excited state. We find that the maximum efficiency occurs when the matrix elements from both ground states have almost the same absolute values. The phase evolution of the different states governs the direction of the population transfer during the pulse. That is why Fig. 11 exhibits a double-peak structure for the intermediate excited states.

Fig. 12 shows the dependence of the spin magnetic moment of the NiO(001) surface with respect to the duration and intensity of the pulse, after the pulse is switched off and the system has reached a static state. The static B-field is perpendicular to the surface and the laser pulse is linearly polarized at a direction parallel to the surface. Contrary to previous works<sup>4,31</sup>, taking into advantage of the breaking of the time reversal symmetry due to the B-field, we find optimal switching conditions for linearly polarized light, more specifically with propagation direction parallel to the static B-field—this is consistent with the experimental findings of Koopmans *et al.*<sup>33</sup> in an experimental setup similar to ours. Our calculations indicate

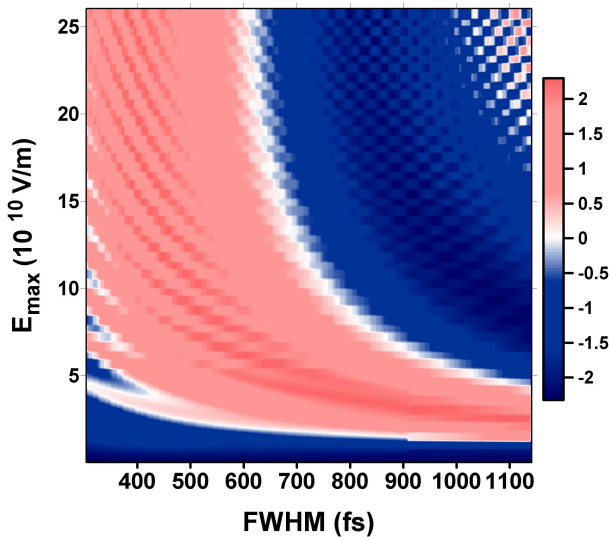


FIG. 12: Contour plot of the final magnetic state of the  $\text{NiO}_5^{-8}$  cluster after the application of a linearly polarized  $\text{sech}^2$ -shaped laser pulse and an external static magnetic field  $B_{\text{ext}} = B_z = 12.5$  A/m vs. duration and intensity of the pulse.

that the use of circularly polarized light can selectively activate one channel of the  $\Lambda$ -process (see inset in Fig. 11), only allowing either excitation or de-excitation, while a superposition of the two polarizations can selectively control the percentage of the population transfer<sup>34</sup>. Similar to our results, Stanciu *et al.* observed subpicosecond magnetization reversal in a ferrimagnetic system, however, with a circularly polarized laser pulse without magnetic field<sup>35</sup>.

Note that breaking of the time-reversal symmetry leads to a differentiation of the roles of  $\langle L^2 \rangle$  and  $\langle L \rangle$ . While the former describes crystalline anisotropy and survives unharmed the existence of the external B-field, the latter one lifts spatial degeneracies and gives rise to dynamic effects of magnetic origin (e.g. Kerr and Faraday effects). Thus linear and quadratic coupling to the (anti)-ferromagnetic order parameters become detectable in optics.

### C. Quantized phonons

In order to consider phonons in a fully quantized picture we first calculate the normal modes of our cluster by diagonalizing the dynamical matrix. Then we quantize the normal modes and subsequently calculate the phonon-electron interaction by fully quantum-mechanically considering  $\frac{\partial \langle \hat{H} \rangle}{\partial q}$ , where  $q$  is the phononic coordinate as seen in Figures 9 and 10<sup>36</sup>. Then we include them together with the SOC and the external static magnetic field in one diagonalization step and therefore to eliminate the problem of applying twice a perturbative method on the wavefunction. Fig. 13 shows the magnetic state of the  $\text{NiO}_6^{-10}$  cluster in the presence of one  $\Gamma$ -point optical phonon after the application of a linearly polarized laser pulse and an external static magnetic field vs. duration and intensity of the pulse. The existence of optical

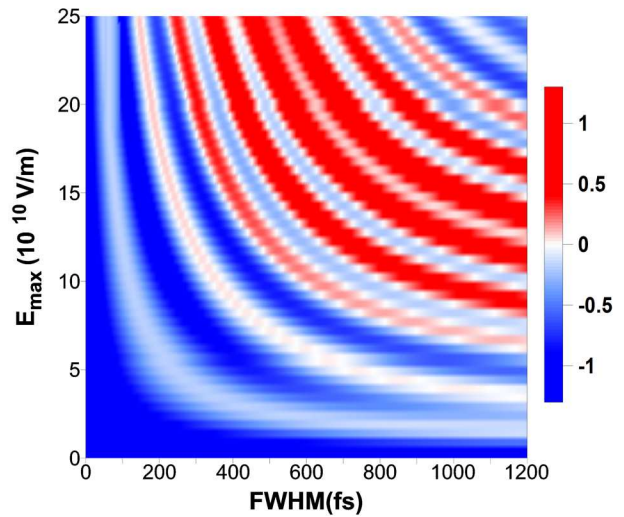


FIG. 13: Contour plot of the magnetic state of the  $\text{NiO}_6^{-10}$  cluster in the presence of one  $\Gamma$ -point optical phonon after the application of a linearly polarized  $\text{sech}^2$ -shaped laser pulse and an external static magnetic field  $B_{\text{ext}} = B_z = 12.5$  A/m vs. duration and intensity of the pulse.

phonons moves the switching parameters towards higher intensities and longer times, while decreasing the tolerance of the system for achieving switching.

Temperature analysis indicates that the elevated lattice temperature makes the effect of switching more efficient, while electronic temperature (loosely defined) does not significantly alter the process, since the first one significantly changes symmetry, while the second one does not<sup>36</sup>.

## VII. SUMMARY AND OUTLOOK

In summary, we have presented a quantum chemistry method for calculating different contributions to SHG both for the bulk and for the (001) surface of NiO, without involving any empirical parameter. We consider not only the ED approximation but MD and EQ induced transitions as well, and we also calculate the phononic effects within the frozen-phonon approximation. It is shown that all of the following, the SOC, the surface, the nonlocal contributions of the laser field, and the transient lattice distortions, can give rise to peaks in the centrosymmetric bulk NiO. The results also indicate the possibility to disentangle the surface (001) from the bulk signal due to different geometrical and frequency dependencies, which has been confirmed in a recent experiment<sup>10</sup>.

We present a fully *ab initio* ultrafast magneto-optical switching mechanism in NiO and show that controlled switching is possible by including SOC in order to take advantage of a  $\Lambda$ -process. The role of phonons is further discussed in a fully quantized picture as a symmetry-lowering mechanism in the switching scenario.

The role of symmetry analysis is definitely significant through the whole paper. It has been used to classify the elec-

tronic states and judge the allowed dipole transitions in SOC, simplify the tensor elements of the high order transitions in SHG, and help us recognize the allowed transitions in the realization of ultrafast switching.

Up to now, we only have considered one magnetic center (one Ni atom) in our investigations. Although the present single-site model can mostly account for AF ordering in NiO (both bulk and surface) because of the high spin density on the Ni sites, it is still necessary to involve more magnetic centers to study more subtle systems for possible applications such as magnetic logic units.

Note that since our calculations were performed on a one-magnetic-center cluster we therefore did not need to consider gauge including atomic orbitals (GIAOs). However, clusters containing more than one active magnetic center should (perhaps) include the phase factor  $e^{i\mathbf{A}\cdot\mathbf{r}}$  in the atomic orbitals.

Although spin is not a good quantum number after the in-

clusion of SOC the breaking of the time-reversal symmetry does not inhibit the calculation of its expectation value. However, it is necessary to account for it in a full spinor basis (two-component) even though rotational invariance is violated in the cluster. For systems where the spin density is localized on one magnetic center only (i.e. NiO) one can consider this center as the origin of the spatial symmetry operations, but for multi-centered clusters the necessity of fully accounting for the spinors becomes imminent.

### Acknowledgements

We would like to acknowledge support from the MINAS Landesschwerpunkt, and Priority Programme 1133 of the German Research Foundation.

- 
- \* Electronic address: chun@physik.uni-kl.de
- <sup>1</sup> E. Beaurepaire, J.-C. Merle, A. Daunois, and J.-Y. Bigot, *Phys. Rev. Lett.* **76**, 4250 (1996).
  - <sup>2</sup> B. Koopmans, J. J. M. Ruigrok, F. D. Longa, and W. J. M. de Jonge, *Phys. Rev. Lett.* **95**, 267207 (2005).
  - <sup>3</sup> J. Chovan, E. G. Kavousanaki, and I. E. Perakis, *Phys. Rev. Lett.* **96**, 057402 (2006).
  - <sup>4</sup> R. Gómez-Abal, O. Ney, K. Satitkovitchai, and W. Hübner, *Phys. Rev. Lett.* **92**, 227402 (2004).
  - <sup>5</sup> A. V. Kimel, A. Kirilyuk, P. A. Usachev, R. V. Pisarev, A. M. Balashov, and T. Rasing, *Nature* **435**, 6558 (2005).
  - <sup>6</sup> T. Lottermoser, T. Lonkai, U. Amann, D. Hohlwein, J. Ihringer, and M. Fiebig, *Nature* **430**, 541 (2004).
  - <sup>7</sup> M. Fiebig, D. Fröhlich, T. Lottermoser, V. V. Pavlov, R. V. Pisarev, and H.-J. Weber, *Phys. Rev. Lett.* **87**, 137202 (2001).
  - <sup>8</sup> G. Lefkidis and W. Hübner, *Phys. Rev. Lett.* **95**, 77401 (2005).
  - <sup>9</sup> K. Satitkovitchai, Y. Pavlyukh, and W. Hübner, *Phys. Rev. B* **72**, 45116 (2005).
  - <sup>10</sup> M. Nývlt, F. Bisio, and J. Kirschner, *Phys. Rev. B* **77**, 14435 (2008).
  - <sup>11</sup> B. Fromme, M. Möller, T. Anschutz, C. Bethke, and E. Kisker, *Phys. Rev. Lett.* **77**, 1548 (1996).
  - <sup>12</sup> A. Gorschlüter and H. Merz, *Phys. Rev. B* **49**, 17293 (1994).
  - <sup>13</sup> R. Newman and R. Chrenko, *Phys. Rev.* **114**, 1507 (1959).
  - <sup>14</sup> A. I. Lichtenstein and M. I. Katsnelson, *Phys. Rev. B* **57**, 6884 (1998).
  - <sup>15</sup> F. Aryasetiawan and O. Gunnarsson, *Phys. Rev. Lett.* **74**, 3221 (1995).
  - <sup>16</sup> S. V. Faleev, M. v. Schilfgaard, and T. Kotani, *Phys. Rev. Lett.* **93**, 126406 (2004).
  - <sup>17</sup> J.-L. Li, G.-M. Rignanese, and S. Louie, *Phys. Rev. B* **71**, 193102 (2005).
  - <sup>18</sup> J. Kuneš, V. I. Anisimov, S. L. Skornyakov, A. V. Lukoyanov, and D. Vollhardt, *Phys. Rev. Lett.* **99**, 156404 (2007).
  - <sup>19</sup> K. Satitkovitchai, Y. Pavlyukh, and W. Hübner, *Phys. Rev. B* **67**, 165413 (2003).
  - <sup>20</sup> M. Head-Gordon, D. Maurice, and M. Oumi, *Chem. Phys. Lett.* **246**, 114 (1995).
  - <sup>21</sup> G. Lefkidis and W. Hübner, *Phys. Rev. B* **74**, 155106 (2006).
  - <sup>22</sup> T. from<sup>8</sup> and the references therein. (????).
  - <sup>23</sup> Y. Tanabe, M. Fiebig, and E. Hanamura, *Magneto-optics* (Springer, 2000).
  - <sup>24</sup> Y. R. Shen, *The Principles of Nonlinear Optics* (John Wiley and Sons, 1984).
  - <sup>25</sup> T. Andersen, O. Keller, W. Hübner, and B. Johansson, *Phys. Rev. A* **70**, 043806 (2004).
  - <sup>26</sup> W. Hübner and K.-H. Bennemann, *Phys. Rev. B* **40**, 5973 (1989).
  - <sup>27</sup> G. Lefkidis, O. Ney, and W. Hübner, *Phys. Stat. Sol. (C)* **2**, 4022 (2005).
  - <sup>28</sup> A. Dähn, W. Hübner, and K. H. Bennemann, *Phys. Rev. Lett.* **77**, 3929 (1996).
  - <sup>29</sup> R. Birss, *Symmetry and Magnetism* (North-Holland Publishing Company, 1964).
  - <sup>30</sup> T. Andersen and W. Hübner, *Phys. Rev. B* **65**, 174409 (2002).
  - <sup>31</sup> R. Gómez-Abal and W. Hübner, *Phys. Rev. B* **65**, 195114 (2002).
  - <sup>32</sup> R. Gómez-Abal and W. Hübner, *J. Phys. Condens. Matter* **15**, S709 (2003).
  - <sup>33</sup> F. D. Longa, C. J. T. Kohlhepp, W. J. M. de Jonge, and B. Koopmans, *cond-mat* p. 0609698 (2006).
  - <sup>34</sup> G. Lefkidis and W. Hübner, *Phys. Rev. B* **76**, 014418 (2007).
  - <sup>35</sup> C. D. Stanciu, F. Hansteen, A. V. Kimel, A. Kirilyuk, A. Tsukamoto, A. Itoh, and T. Rasing, *Phys. Rev. Lett.* **99**, 047601 (2007).
  - <sup>36</sup> G. Lefkidis and W. Hübner, *J. Magn. Magn. Mater.* (in press).